MOLECULAR CANCER BIOLOGY

Basal-like mammary carcinomas stimulate cancer stem cell properties through AXL-signaling to induce chemotherapy resistance

Garyfallia Pantelaiou-Prokaki [1,2] | Oliver Reinhardt [1] | Nadine S. Georges [2] |
David J. Agorku [3] | Olaf Hardt [3] | Evangelos Prokakis [2] |
Iga K. Mieczkowska [4] | Wolfgang Deppert [5] | Florian Wegwitz [2,4] |
Frauke Alves [1,6,7]

[1]Max Planck Institute for Multidisciplinary Sciences, Translational Molecular Imaging, Göttingen, Germany

[2]Department of Gynecology and Obstetrics, University Medical Center Göttingen, Göttingen, Germany

[3]Miltenyi Biotec B.V. & Co. KG, R&D Reagents, Bergisch Gladbach, Germany

[4]Department of General, Visceral and Pediatric Surgery, University Medical Center Göttingen, Göttingen, Germany

[5]University Medical Center Hamburg Eppendorf, Institute for Tumor Biology, University of Hamburg, Hamburg, Germany

[6]Institute for Diagnostic and Interventional Radiology, University Medical Center Göttingen, Göttingen, Germany

[7]Clinic for Hematology and Medical Oncology, University Medical Center Göttingen, Göttingen, Germany

Correspondence
Frauke Alves, Translational Molecular Imaging, Max Planck Institute for Multidisciplinary Sciences, Hermann Rein Str. 3, 37075 Göttingen, Germany.
Email: falves@gwdg.de

Florian Wegwitz, Department of Gynecology and Obstetrics, Laboratory for Molecular Gynecology, University Medical Center Göttingen, Georg-August-University, Robert-Koch-Straße 40, 37075 Göttingen, Germany.
Email: fwegwit@gwdg.de, florian.wegwitz@med.uni-goettingen.de

Abstract

Basal-like breast cancer (BLBC) is the most aggressive and heterogeneous breast cancer (BC) subtype. Conventional chemotherapies represent next to surgery the most frequently employed treatment options. Unfortunately, resistant tumor phenotypes often develop, resulting in therapeutic failure. To identify the early events occurring upon the first drug application and initiating chemotherapy resistance in BLBC, we leveraged the WAP-T syngeneic mammary carcinoma mouse model and we developed a strategy combining magnetic-activated cell sorting (MACS)-based tumor cell enrichment with high-throughput transcriptome analyses. We discovered that chemotherapy induced a massive gene expression reprogramming toward stemness acquisition to tolerate and survive the cytotoxic treatment in vitro and in vivo. Retransplantation experiments revealed that one single cycle of cytotoxic drug combination therapy (Cyclophosphamide, Adriamycin and 5-Fluorouracil) suffices to induce resistant tumor cell phenotypes in vivo. We identified

Axl and its ligand *Pros1* as highly induced genes driving cancer stem cell (CSC) properties upon chemotherapy in vivo and in vitro. Furthermore, from our analysis of BLBC patient datasets, we found that *AXL* expression is also strongly correlated with CSC-gene signatures, a poor response to conventional therapies and worse survival outcomes in those patients. Finally, we demonstrate that AXL inhibition sensitized BLBC-cells to cytotoxic treatment in vitro. Together, our data support AXL as a promising therapeutic target to optimize the efficiency of conventional cytotoxic therapies in BLBC.

KEYWORDS
AXL, basal-like breast cancer, breast cancer stem cell, chemoresistance, syngeneic mouse model

What's new?
Basal-like breast cancer (BLBC) is the most aggressive breast cancer subtype, and it often develops resistance to chemotherapy. Here, the authors used high-throughput mRNA sequencing to identify transcriptional changes that allowed the tumor cells to withstand chemotherapy. After only one round of combination chemotherapy (Cyclophosphamide, Adriamycin and 5-Fluorouracil) the tumor cells had begun a massive gene expression reprogramming, becoming more like cancer stem cells by activating *Axl* and its ligand *Pros1*. They also showed that inhibition of AXL made the cells susceptible to cytotoxic treatment in vitro, suggesting AXL may be a potential therapeutic target.

1 | INTRODUCTION

Breast cancer (BC) is the most common malignancy with the second highest mortality rate in women worldwide.[1] Due to its heterogeneous nature, BC has been classified into different subtypes based on the expression of estrogen receptor (ER), progesterone receptor (PR) and human epidermal growth factor 2 (HER2) receptor evaluated by immunohistochemistry (IHC). Therapies specifically targeting the activity of these receptors have considerably improved the survival outcomes of luminal A (ER$^+$/PR$^+$, HER2$^-$), luminal B (ER$^+$/PR$^+$, HER2$^{+/-}$) and HER2$^+$ (ER$^-$/PR$^-$, HER2$^+$) BC patients.[1] In stark contrast, 10% to 15% of all BC lesions do not express any of these receptors and are, therefore, classified as triple-negative BC (TNBC). This subtype largely overlaps with the basal-like breast cancer (BLBC) molecular subtype and unfortunately does not profit from therapies targeting the hormone- and HER2 receptors.

TNBC lesions are generally treated with a neoadjuvant combination of taxane- and anthracycline-based combination chemotherapies, while platinum-based chemotherapy has shown promising results, among others in metastatic disease treatments.[2] Despite good early response to such therapies, 40% of the treated patients develop recurrence arising close to the primary tumor site or as metastasis in distant parts of the body, including the lung and bone marrow.[3,4] Therefore, in most cases, conventional therapies (chemotherapy, radiotherapy) remain next to surgical resection as the only therapeutic approach and novel therapeutic targets are urgently needed.[5]

Previous studies demonstrated that chemotherapy can induce tumor cell reprogramming, conferring proliferation advantages, and promoting a switch from a transient drug-tolerant state to an irreversible drug-resistant state leading to tumor recurrence.[6-9] Chemotherapy-resistant breast cancer lesions often enrich for cells with high CD44 (cluster of differentiation 44) expression, low levels of CD24 (cluster of differentiation 24) and/or high aldehyde dehydrogenase activity (ALDH^{high}), the so-called breast cancer stem cells (BCSC).[7,10,11] Interestingly, these particular tumor cells were associated with enhanced self-renewal and prosurvival properties, but also showed improved drug resistance and chemotherapeutic agents efflux. Therefore, BCSCs are thought to be largely involved in premature tumor relapse development.[12-14]

To date, the precise kinetic underlying the development of resistant phenotype during cyclic chemotherapy treatment regimen is insufficiently understood. A better knowledge of the sequential cellular events responsible for the acquisition of chemoresistance is of utmost importance to predict the gradual loss of therapy efficiency and identify adequate time points for therapeutic refinement. In the present study, we investigated the transcriptional changes following one single combination chemotherapy (Cyclophosphamide, Adriamycin, 5-Fluorouracil [CAF]) administration on tumor cells in vivo. We leveraged the WAP-T mouse model as a useful surrogate of human BLBC.[15-17] Upon orthotopic transplantation in syngeneic animals, WAP-T tumor cell lines generate poorly differentiated basal-like breast tumors harboring a high degree of epithelial-mesenchymal plasticity.[15,18,19] This model was successfully utilized in the past to study polycomb repressive complex 2 (PRC2) and histone deacetylase 8 (HDAC8) mediated epigenetic mechanisms during the acquisition of resistance to various cytotoxic drugs.[20,21] Chemotherapy treatment of WAP-T tumors only transiently reduces the volume of the lesions and tumors regrow after a few days.[22] In the present study, we demonstrate that WAP-T tumor cells experiencing one CAF treatment cycle in vivo had already gained therapy resistance in retransplantation

experiments. We analyzed the transcriptional changes occurring in chemotherapy-surviving tumor cells in vivo, applying an advanced combination of magnetic cell sorting-based tumor cell enrichment and high throughput mRNA-sequencing (mRNA-seq). We discovered that the acquisition of stem cell properties is an early event in response to chemotherapies promoting tumor evolution to resistant phenotypes. Our investigations identified *Axl*, a member of the TYRO3, AXL, MERTK (TAM) tyrosine kinase receptor family, as one of the most prominently induced genes upon chemotherapy and established its crucial implication in the acquisition of CSC-mediated drug-resistance properties.

2 | MATERIALS AND METHODS

2.1 | Cell lines and animal model

H8N8[15,23] and its derivatives T1 (untreated), T2 (CAF-survived) and T3 (CAF-regrowth) were maintained in high Glucose (4.5 g/L D-Glucose) Dulbecco's modified Eagle's medium (DMEM, Thermo Fisher Scientific Corp., Waltham, MA) containing 10% fetal calf serum (FCS, Thermo Fisher Scientific Corp., Waltham, MA) at 37°C in a humidified atmosphere with 5% CO_2. All experiments were performed with mycoplasma-free cells. WAP-T animals were kept and treated according to German regulations for animal experiments. See Data S1 for in vivo experiments and for Table S1.

2.2 | Chemotherapy treatment in BLBC models

2.2.1 | In vivo

CAF chemotherapy was performed using 100 mg/kg body weight (BW) cyclophosphamide (Endoxan, Baxter, Deerfield, IL), 5 mg/kg BW doxorubicin (Cell Pharm, Hannover, Germany) and 100 mg/kg BW 5-fluorouracil (5-FU) (Medac, Wedel, Germany)[22] (See Data S1 for in vivo experiments and for Table S6).

2.2.2 | In vitro

A detailed table with CAF composition at different dilutions is given in Table S6. The different chemotherapies were applied to the cells for 1 cycle/48 hours in synergy assays and for 2 cycles/24 hours, one before and one after silencing of *Axl* and *Mertk* in dose-response assays, respectively.

2.3 | Histology

Tissue specimens for histology were fixed in formalin, embedded in paraffin, cut into sections of 5 μm and deparaffinized. A Masson trichrome kit (MTS, Merck, Darmstadt, Germany) was used to stain collagen. Histological H&E, as well as immunostaining of CD44 and AXL were performed as previously published.[24] Primary and secondary antibody dilutions, as well as individual conjugations, are listed in Table S2.

2.4 | Dissociation of tumor tissue, flow cytometry and tumor cell isolation

Fresh mouse tumor tissue was dissociated and analyzed by flow cytometry. Untreated and CAF-treated H8N8 tumor cells were extracted and isolated from the growing tumors and depletion of nontumor cells was performed by magnetic-activated cell sorting (MACS) using CD45 (TIL), MicroBeads and the mouse Tumor Cell Isolation Kit (Miltenyi Biotec, Bergisch Gladbach, Germany) according to the manufacturer's instructions. For flow cytometric analysis, single-cell suspensions were stained with the indicated antibodies (Table S3) and analyzed using the MACSQuant Analyzer 10 (all Miltenyi Biotec, Bergisch Gladbach, Germany). The purity analysis procedure of isolated tumor cells is provided in the Data S1.

2.5 | siRNA transfection

Cells were reverse transfected with siRNA using Lipofectamine RNAiMAX, according to the manufacturer's instructions. siGENOME siRNAs (Dharmacon) were acquired at Horizon Discovery Ltd and utilized as smart pools of four different siRNAs equimolarly mixed (each 5 μM). siRNAs: Non-targeting control #5 (NT5) [D-001210-05-05], murine *Axl* [MQ-040941-01-0002], murine *Mertk* [M-040357-00-0005].

2.6 | Inhibitor and recombinant protein treatment

For RTK inhibition/stimulation in H8N8 cells, 2 cycles of 48 hours of treatment with R428 (AXL inhibitor, AdooQ, cat. No. A13741), UNC2250 (MERTK inhibitor, MedChemExpress, cat. HY-15797), rPROS1 (R&D systems, cat. 9740-PS-050) or rGAS6 (SinoBiological, cat. 58026-M08H) were performed. Chemotherapy treatment was performed together with the first cycle of inhibition/stimulation, 24 hours after cell seeding.

2.7 | Proliferation assay

2.7.1 | 96-well format

2000 to 3000 cells per well were seeded. For inhibitor/stimulation experiments, the treatment scheme is provided in the previous section. For knockdown experiments, 24 hours after seeding, cells were treated for 24 hours with the first cycle of CAF, followed by siRNA transfection. Twenty-four hours later, the second cycle of CAF was performed for a duration of 24 hours. The confluence was measured using an Incucyte Live-Cell Analysis System (Sartorius, Germany).

2.7.2 | 24-well format

10 000 cells per well were seeded. On the last day of the experiment, cells were fixed with 100% methanol for 10 minutes and stained using

crystal violet for 20 minutes. The cell layer confluence was estimated with ImageJ (version 1.53f51).

Synergy analyses were performed using SynergyFinder (https://synergyfinder.fimm.fi/synergy/20220802115600588518/).

2.8 | Colony and tumorsphere formation assays

2.8.1 | Colony formation assay

1000 cells per well were seeded in a 6-well plate. On the last day of the experiment, cells were fixed with 100% methanol for 10 minutes and stained using crystal violet for 20 minutes. The median colony size of H8N8 cells was estimated with ImageJ (version 1.53f51).

2.8.2 | Tumorsphere formation assay

1000 cells per well were seeded in a low-adherent 96-well plate. Cells were treated with AXL inhibitor (R428) and with chemotherapy for 48 hours before seeding in a low-adherent 96-well plate. Spheres were imaged using a Celigo Cell Cytometer device (Nexcelom Bioscience, UK). The number of spheres was estimated with ImageJ (version 1.53f51).

2.9 | Immunofluorescence staining and imaging

Immunofluorescence staining was performed as previously published.[25] For detailed protocol, refer to Data S1.

2.10 | Tumor cell RNA isolation, mRNA library preparation and sequencing

2.10.1 | mRNA extraction

mRNAs were isolated using QIAzole (Qiagen AG, Hilden, Germany) from cell pellets with 1×10^6 cells each. The quality of the mRNAs was examined with an Agilent 2100 Bioanalyzer (Agilent Technologies, Santa Clara, CA) using the Agilent RNA 6000 Nano Kit (Agilent Technologies, Santa Clara, CA).

2.10.2 | Library generation and sequencing

mRNA sequencing libraries were generated using the NEXTflex Rapid Directional RNA-Seq Library Prep Kit (Bioo Scientific, Austin, TX) and sequenced in a HiSeq 4000 sequencer (Illumina, San Diego, CA) at the NIG (NGS Integrative Genomics Core Unit, University Medical Center Göttingen).

2.10.3 | Gene set enrichment analysis

Gene Set Enrichment Analyses (GSEA, v.4.1.0) were performed using the following settings: Number of permutations = 1000; Collapse to gene symbols = No_Collapse; Permutation type = gene_set, metric for ranking genes = Signal2Noise; Max size = 5000; Min size = 15. Gene set database used in our study: Hallmarks (v. 7.4) and C2 Curated gene sets (v. 7.4, chemical and genetic perturbations).

2.10.4 | Differential expression analyses

The DESeq2 tool (v. 2.11.40.6 + galaxy1) was utilized in the Galaxy environment provided by the Gesellschaft für wissenschaftliche Datenverarbeitung mbH Göttingen (GWDG) to calculate changes of gene expression in the different mRNA-seq datasets.

Radar-plot in Figure 3D was designed using Origin 2022 (v. 9.9.0.220).

Detailed tumor cell *RNA isolation*, *library preparation*, *sequencing extraction procedure* and *mRNA-seq data analysis* workflow are provided in the Data S1. Also, sequencing coverage and quality statistics of the RNA sequencing generated in our study are summarized in Table S7.

2.11 | Publically available data

2.11.1 | Homemade gene set "AXL_DN_GENES_DN"

mRNA-seq data of MDA-MB-231 were retrieved from Gene Expression Omnibus (GEO) under the accession number GSE120268. The homemade gene set "AXL_DN_GENES_DN" was generated using the following cut-offs from the respective DESeq2 file: basemean ≥15, log2FC ≤−0.7, *P*-val <.05.

2.11.2 | Patient survival analyses

Patient survival data were retrieved from The Cancer Genome Atlas (TCGA, xenabrowser.net) platform to examine the association of *AXL* (OS: cut-off = 10.54) average expression with patient survival in BLBC patients. The *AXL* expression cut-off was selected using the CutoffFinder (v1, https://molpathoheidelberg.shinyapps.io/CutoffFinder_v1/). Receiver operating characteristic (ROC) analysis of TNBC patients based on *AXL* expression (id: 202685_s_at) was performed using a ROC plotter (http://www.rocplot.org/site/treatment).

2.12 | cDNA synthesis

The reverse transcription of mRNAs-samples was performed using the First Strand cDNA Synthesis Kit (M-MLuV, NEB, UK) according to the manufacturer's instructions. Briefly, 1 μg of RNA was diluted to a

total volume of 10 μL with RNase-free water and mixed with 2 μL of random 9mer primers (60 μM) and 1 μL of dNTPs (10 mM). The mixture was incubated for 5 minutes at 65°C and thereafter immediately transferred on ice. Next, 2 μL of ×10 M-MuLV buffer, 0.2 μL RNase inhibitor (40 U/μL), 1 μL M-MuLV reverse transcriptase (200 U/μL) and 6.8 μL diethylpyrocarbonate (DEPC) water were added, gently mixed, incubated at 25°C for 5 minutes and then at 42°C for 60 minutes. To inactivate the reverse transcriptase, samples were finally heated for 20 minutes at 65°C. The reaction mixture was diluted to a total volume of 200 μL and stored at −20°C.

2.13 | Quantitative real-time polymerase chain reaction

For quantitative real-time polymerase chain reaction (qRT-PCR), 1 μL of diluted cDNA (see the previous section) and 10 pmol of each primer

were utilized per reaction in 25 μL total volume (homemade SYBR-green qPCR master mix). Samples were run with the following amplification program: 95°C for 2 minutes, 40 cycles (95°C for 15 seconds, 60°C for 30 seconds) in a BioRad CFX96 system (USA). A melting curve analysis was subsequently generated (67°C-95°C, 0.5°C/second). Samples were quantified by using the method of the standard curve. The samples were normalized to the *Rplp0* housekeeping genes. A list of primers used in our study is available in Table S4.

2.14 | Western blotting

Proteins were extracted from 6-wells plates with 500 μL ice-cold RIPA buffer following the standard procedure established in our lab.[24] Equal amounts of samples were separated using 10% to 12% SDS polyacrylamide gel electrophoresis and transferred onto nitro-cellulose membranes (Immobilon, Millipore, USA). After incubation
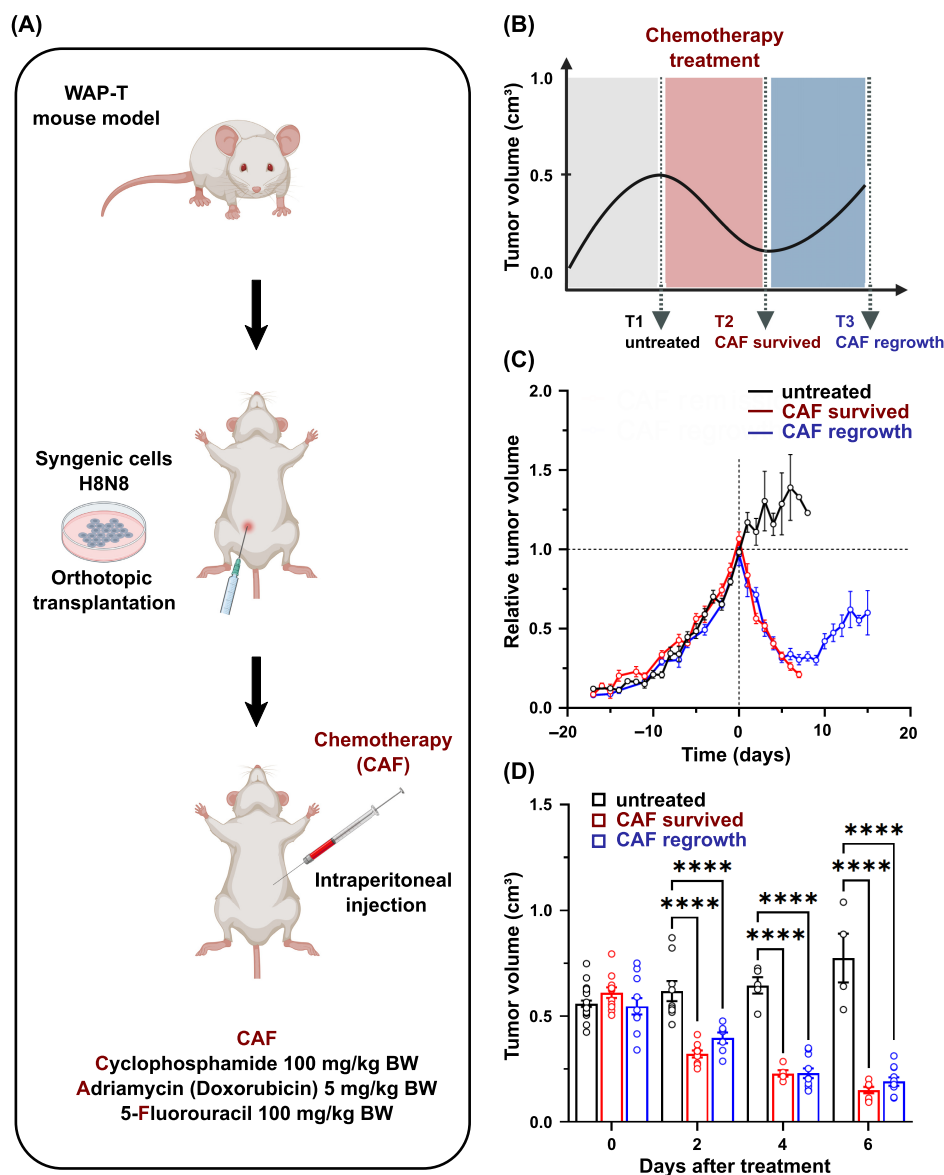
FIGURE 1 Temporary remission of H8N8 tumors in response to one-dose CAF chemotherapy. (A) Schematic representation of the animal experimental procedures: H8N8 tumor cell cultivation, transplantation in female non-induced transgenic heterozygous WAP-T mice and CAF application. (B) Groups of untreated and CAF-treated tumor-bearing mice are depicted. (C) Tumor growth kinetics of untreated and CAF-treated H8N8 tumors are shown. Tumor volumes were normalized to the mean of the tumor volumes of all tumors (dashed horizontal line) at the start of therapy (day 0) and then averaged. Tumor volumes were measured in situ on live mice by caliper measurements (untreated n = 22, CAF-survived n = 11 and CAF-regrowth n = 11). Data from two independent experiments. (D) Tumor volumes of the untreated H8N8 tumors were compared to those treated with CAF, from day zero to six after CAF application. *P*-values were calculated by 2-way ANOVA Bonferroni's multiple comparisons tests. ****$P < .001$. Day 0 marks the time of CAF administration and thus the time of a tumor volume of ∼500 mm^3 (untreated n = 22 and CAF n = 22). BW, body weight
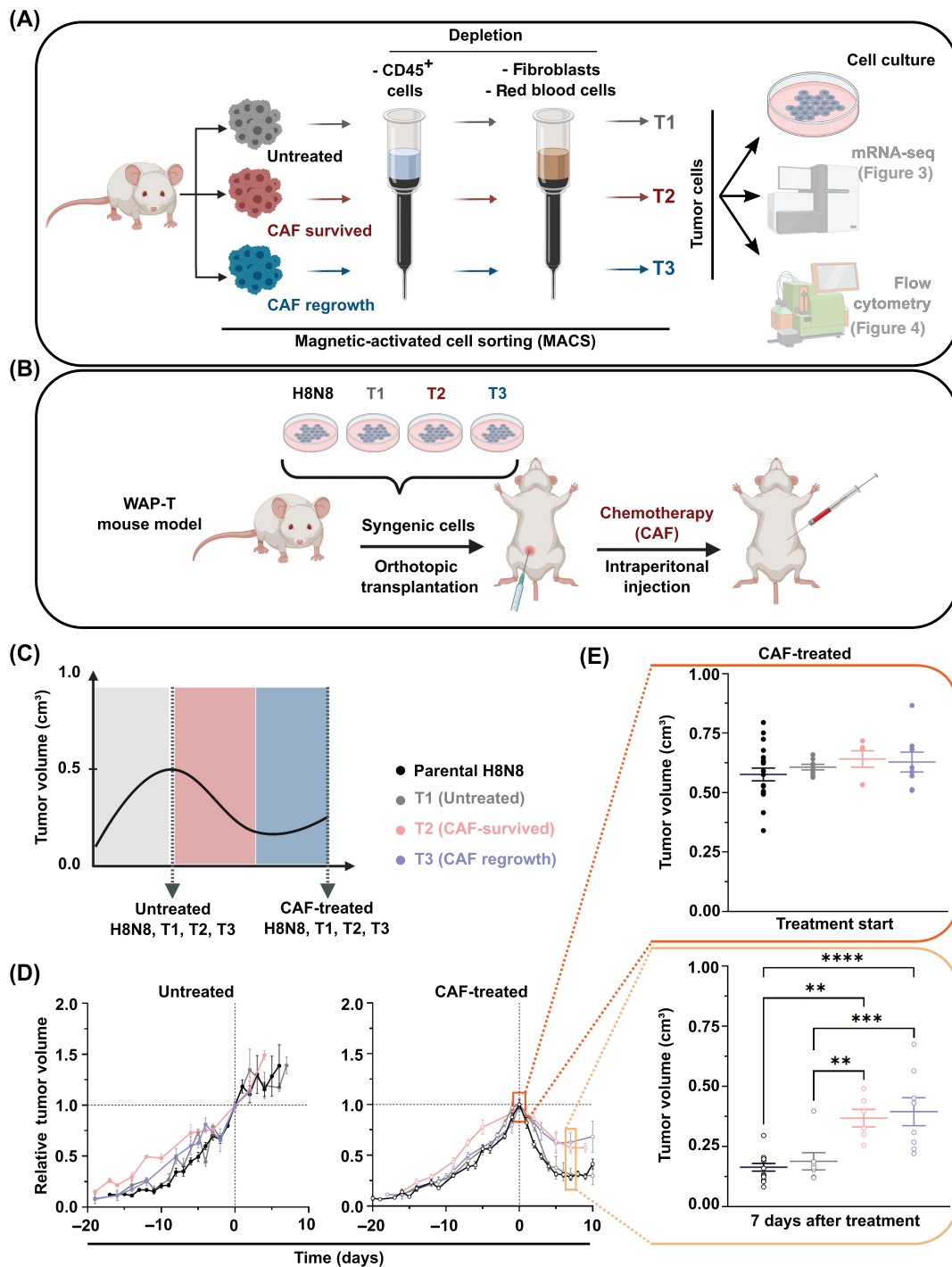
FIGURE 2 Single-cell sorting of CAF-treated tumors showed particularly aggressive behavior in orthotopically retransplanted mice with renewed CAF therapy. (A) The workflow for tumor cell enrichment from dissociated suspensions of bulk tumors by immunomagnetic sorting. In the first step, CD45-expressing cells were labeled and magnetically isolated. From the leukocyte-depleted fraction, the tumor cells were then isolated by labeling and magnetically depleting the remaining nontumor cells, such as stromal and red blood cells. (B) Schematic representation of the animal experimental procedures: (re-)transplantation of H8N8, T1 (untreated), T2 (CAF-survived) and T3 (CAF-regrowth) tumor cells in females non-induced transgenic heterozygous WAP-T mice and CAF application. (C) Groups and CAF treatment regimens are depicted. (D) Tumor growth kinetics of untreated (left), and CAF treated (right) H8N8, T1 (untreated), T2 (CAF-survived) and T3 (CAF-regrowth) tumors are displayed. The tumor volumes were normalized to the mean of the tumor volumes of all tumors from the same group (dashed horizontal line) at the start of therapy (day 0) and then averaged. Tumor volumes were measured in situ on living mice by caliper measurements (untreated: H8N8 n = 22, T1 n = 6, T2 n = 4 and T3 n = 5; CAF-treated: H8N8 n = 19, T1 n = 8, T2 n = 6 and T3 n = 8). (E) Absolute tumor volumes of the CAF-treated H8N8, T1, T2 and T3 tumors are shown, from the treatment start (upper, orange square) and 7 days after treatment (lower, yellow square). P-values were calculated by ordinary one-way ANOVA Turkey's multiple comparisons tests. **$P < .01$, ***$P < .005$ and ****$P < .001$

with the first antibody and the HRP-coupled secondary antibody (listed in Table S5), the membranes were developed in a ChemoStar imaging system (INTAS science imaging, DE). A detailed protocol is provided in the Data S1.

2.15 | Statistical analysis

All statistics and final plots were obtained using GraphPad Prism v8.0.1 software. Depending on the nature of the compared datasets,
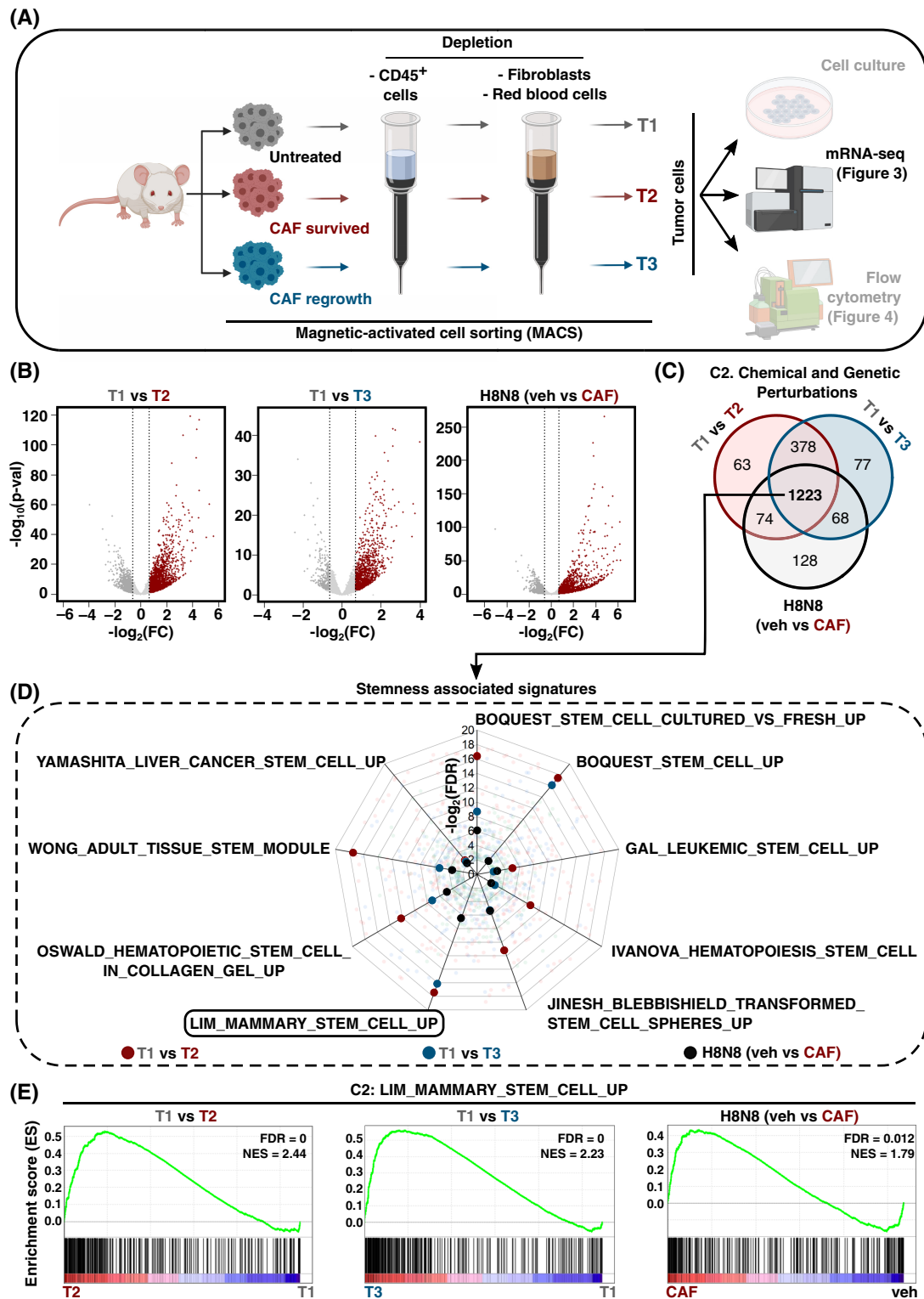
FIGURE 3 Legend on next page.

the following statistical tests were performed: 2-way ANOVA Bonferroni's multiple comparisons tests, ordinary one-way ANOVA Turkey's multiple comparisons tests and 2-way ANOVA Turkey's multiple comparisons tests. In all graphs: P-values: *$P < .05$, **$P < .01$, ***$P < .005$ and ****$P < .001$.

3 | RESULTS

3.1 | Orthotopically transplanted WAP-T mice upon chemotherapy treatment mimic the tumor recurrence in BLBC patients

To study the effect of one cycle of conventional chemotherapy, a combination of CAF, on the growth kinetics of murine BLBC tumors, we employed the well-characterized murine H8N8 tumor cell line orthotopically transplanted in syngeneic immunocompetent WAP-T recipient mice (Figure 1A). Mammary tumors developed and reached a volume of 500 mm^3 within ~30 days. Tumor-bearing mice were divided into three groups: untreated, CAF-survived and CAF-regrowth. Untreated mice were dissected at a tumor volume of ~500 to 1000 mm^3. Mice of the CAF-survived group were treated with one cycle of CAF (100 mg/kg body weight (BW) cyclophosphamide, 5 mg/kg BW doxorubicin, 100 mg/kg BW 5-FU) at a tumor volume of 500 mm^3 and dissected 6 days later (time point where the maximum regression was observed). Mice of the CAF-regrowth group were treated with CAF at a tumor volume of 500 mm^3 as well and were dissected once regrowing tumors reached a maximum volume of ~500 to 1000 mm^3 (Figure 1B). The growth kinetics of the H8N8 tumors in the different groups are provided in Figure 1C. CAF therapy temporarily reduced the tumor volume by 36% and 62% on days two and four after CAF administration, respectively, compared to the untreated tumors. The maximum measured reduction was by 6 days after CAF administration by 76% compared to the untreated tumors. (Figure 1D). The residual tumors started to re-grow after 6 to 8 days and returned to about half of their initial tumor volume 14 days after the CAF application (Figure 1C).

The accuracy of the tumor volume measurements was validated by plotting caliper measured dimensions against the tumor weights at dissection (Figure S1A). The average body weight of treated mice (groups 2 and 3) decreased by 15.2% (±5.1%) within the first 6 days

and reached a maximum of 24.1% (±6.4%) on day 14 after CAF application. In contrast, untreated tumor-bearing mice showed no significant weight change during disease progression (Figure S1B). Together, the selected system closely mimics the situation of recurrences frequently observed in BLBC patients receiving the conventional chemotherapy regimen.

3.2 | Cancer cells developed resistance to CAF therapy

We wondered if tumors regrowing after one chemotherapy dose had already acquired therapy-resistant traits. To study changes in tumor cell phenotype, we opted for an enrichment procedure based on magnetic-activated cell sorting (MACS) to specifically isolate tumor cells from the tumor bulk and unravel the responsible mechanisms driving drug tolerance (Figure 2A). Leukocytes and other nontumor cells were sequentially depleted from the tumor cell fraction by magnetic cell sorting. Subsequently, the purified tumor cells were then utilized to establish cell lines (untreated → T1, CAF-survived → T2, CAF-regrowth → T3), for next-generation sequencing (NGS) and flow cytometry analysis (FC; Figure 2A).

To first examine the capacity of T1 (untreated), T2 (CAF-survived) and T3 (CAF-regrowth) cells to respond to a new dose of CAF therapy in vivo, we orthotopically retransplanted these cells as well as the original H8N8 cells into WAP-T mice (Figure 2B, Table S1). After tumor development, mice of the control and chemotherapy groups were treated with either vehicle or one dose of CAF therapy, respectively, as tumors reached 500 mm^3 and dissected at the maximal size of 1000 mm^3 (Figure 2C). The resistant behavior of the different variants was assessed by measuring the tumor growth kinetics. All investigated groups developed breast tumors up to a size of ~500 mm^3 within 30 days, similar to the growth kinetics of the original H8N8 tumors (Figure 2D, left panel). As expected, naïve tumors from the transplanted H8N8 and retransplanted T1 groups (both never exposed to CAF) showed marked shrinkage in response to CAF treatment (Figure 2D, right panel and Figure 2E). Interestingly, in tumors derived from previously CAF-treated tumor cells (CAF-survived-T2 and CAF-regrowth-T3) an increased drug tolerance to this renewed CAF application was observed (Figure 2D, right panel

FIGURE 3 mRNA-seq of chemotherapy-treated murine MACS-isolated BLBC cells strikingly enrich for stemness properties. (A) Schematic representation of next-generation sequencing of tumor cells enriched by MACS. (B) Volcano plot showing differentially expressed genes in untreated tumor cells vs tumor cells in CAF-survived (left) and vs tumor cells in CAF-regrowth (middle) as well as in vitro untreated H8N8 cells vs CAF-treated H8N8 cells (right). The $-\log_{10}$ (P-values) were plotted against the $\log_2$ fold change gene expression (n = 4 biological replicates of untreated, CAF-survived and CAF-regrowth cells, and n = 3 biological replicates of untreated-H8N8 cells and CAF-treated H8N8 cells). (C) Venn diagram showing the GSEA profiles from the curated gene set collection "C2: chemical and genetic perturbations" of CAF-survived (T2) vs untreated cells (T1), CAF-regrowth (T3) vs untreated cells (T1) and CAF-treated H8N8 cells vs vehicle H8N8 cells. (D) Spider plot showing common stemness-associated signatures in CAF-survived, CAF-regrowth and CAF-treated H8N8 cells ($-\log_2$[FDR] > 2). (E) GSEA profiles showing an enrichment of the "LIM_MAMMARY_STEM_CELL_UP" signature (MSigDB: C2 curated gene sets) in CAF-survived (T2) and CAF-regrowth (T3) compared to untreated (T1) cells, and in H8N8 cells at basal state (control) compared to CAF-treated cells. NES, normalized enrichment score
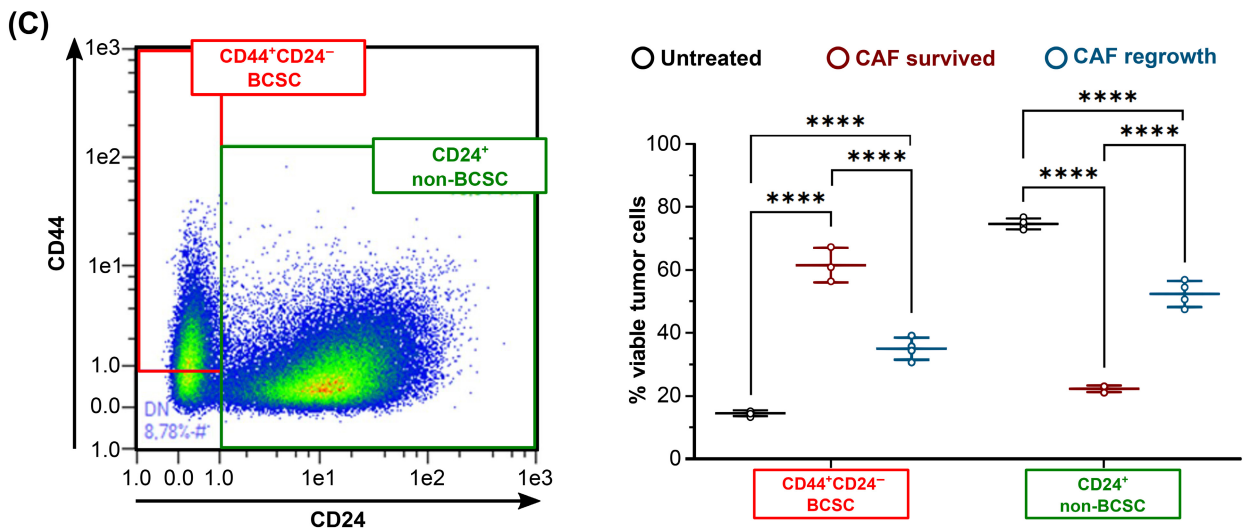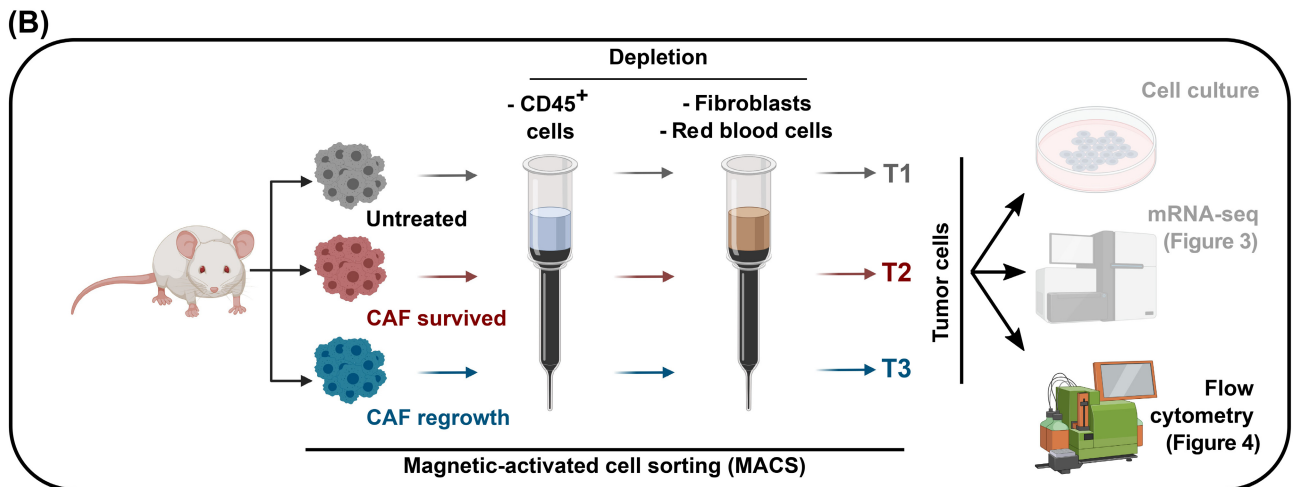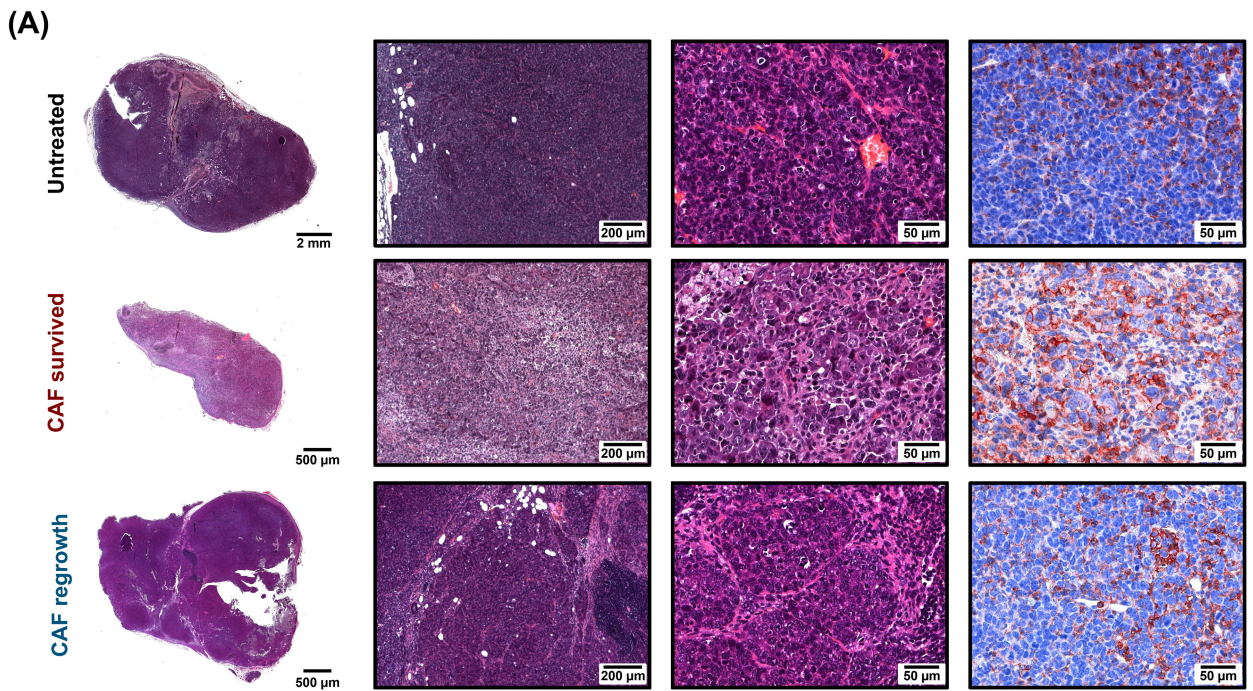
FIGURE 4   Legend on next page.

and Figure 2E). Altogether, these findings support the acquisition of a chemotherapy-resistant phenotype of BLBC cancer cells already after a single dose of chemotherapy in vivo.

3.3 | Tumor cells in remission and regrowth share gene expression properties characteristic of BCSC

We wanted to understand the transcriptomic changes that allowed the acquisition of resistance in the surviving (CAF-survived, T2) and regrowing (CAF-regrowth, T3) tumor cells upon the first chemotherapy. We performed mRNA-seq on purified tumor cells from the different groups as well as on H8N8 cells treated with CAF in vitro (Figures 3A and S1C,D). Surprisingly, the majority of the differentially regulated genes in chemotherapy-treated groups were upregulated (Figure 3B). To identify the gene expression programs driving chemotherapeutic resistance and tumor relapse upon chemotherapy treatment, we performed a gene set enrichment analysis (GSEA) and subsequently intersected all enriched gene sets of the C2 dataset (chemical and genetic perturbation) in T2 (CAF-survived), in T3 (CAF-regrowth) and CAF-treated H8N8 cells. 1223 gene sets were simultaneously enriched in the three groups (Figure 3C). Interestingly, we noticed a strong enrichment for several stem cell-like associated gene expression signatures not only during the acute phase of CAF treatment (H8N8, T2) but also upon regrowth (T3) (Figure 3D). Strikingly, among several CSC-associated gene signatures, the "LIM_MAMMARY_STEM_CELL_UP" gene set was significantly enriched, strongly arguing for a pronounced mammary CSC repopulation in all-time points after chemotherapy treatment (Figure 3D,E). Therefore, CAF chemotherapy induced a massive gene expression reprogramming towards stemness acquisition to tolerate and survive the cytotoxic treatment in vitro and in vivo.

3.4 | Histological and cytometric characterization confirms the chemotherapy-induced emergence of a stemness-associated cancer cell population in BLBC tumors

As the acquisition of stemness-associated properties is a driving force toward chemotherapeutic tolerance and tumor recurrence in several cancer entities,[26] we decided to investigate the expression of markers

associated with CSC traits. Interestingly, hematoxylin and eosin (H&E) stained paraffin sections of CAF-survived and CAF-regrowth tumors showed an increased fraction of stroma tissue compared to untreated controls (Figure 4A) which was confirmed by Masson's trichrome staining (MTS; Figure S1E-G). As the CD44 surface marker expression is associated with stem cell phenotypes, we performed immunohistochemical staining and demonstrated a strong elevation of CD44$^+$ cells in the tumors of the remission phase (CAF-survived). Interestingly, the number of CD44$^+$ cells decreased upon tumor regrowth, pointing to a possible replenishment of the tumor bulk with more differentiated tumor cells (Figure 4A). To further support the increased stemness of surviving tumor cells, we performed a flow cytometry analysis (FC) of the purified tumor cells stained with CD44 and the differentiation marker CD24 using a flow cytometric approach (Figure 4B,C, left panel). Indeed, the number of CD44^{high}/CD24^{low} cells was strongly increased in CAF-survived tumors and dropped in CAF-regrowth tumors but remained at significantly higher levels than in the untreated lesions (Figure 4C, right panel). In contrast, the fraction of cells considered as more differentiated (CD24^{high}) showed the opposite behavior, being strongly decreased in the acute treatment phase and only partially rescued in the regrowth phase (Figure 4C, right panel). Concordantly, FC analysis performed on an additional panel of stem cell-like markers (Cd95, Cd104, Cd146, Cd201 and Sca1) as well as on the differentiation marker Cd107 indicated a similar increase of CSC in CAF-survived and -regrowth tumor tissue (Figure S2A). In agreement, a closer analysis of differentially regulated genes in our mRNA-seq datasets revealed that numerous stemness-associated markers (*Sox2*, *Myc*, *Klf4*, *Nanog*, *Itgb1* and *Abcg2*) were highly increased in tumor cells during the acute treatment phase in vivo as well as in vitro (Figure S2B,C). Overall, these results point to the dynamic behavior of BLBC cancer stem cells whose abundance massively increases in tumors during the acute phase of chemotherapy treatment and remains pronouncedly elevated in the regrowing tumors.

3.5 | AXL is highly associated with a stem cell-like phenotype in chemotherapy-surviving and relapsed BLBC tumors

To identify drug targets that could be leveraged for counteracting the induction of CSC-phenotypes and thereby potentiating the

FIGURE 4 Histological and cytometric characterization of CAF-treated murine TNBC tumors indicates a strong enrichment of CSCs. (A) Representative images of H&E (left: whole section, middle: different magnification, overview and detail) and anti-CD44 (right) staining of paraffin-embedded sections of an untreated tumor (n = 18), a tumor of CAF-survived (n = 8) and one of CAF-regrowth (n = 6). Scale bars of H&E-whole section images correspond to 2 mm, H&E-overview images to 200 μm or 500 μm (CAF-survived and CAF-regrowth), H&E-detail images and CD44 IHC to 50 μm. (B) Schematic representation of flow cytometry of tumor cells enriched by MACS. (C) Representation of the gating strategy for BCSC (CD44$^+$CD24$^-$ marked brown) and non-BCSC (CD24$^+$ marked green) tumor cell population. Tumor cells were magnetically isolated before flow cytometric analysis, cell debris, PI-stained dead cells and possibly remaining magnetically labeled nontumor cells (via Labeling Check Reagent-staining) were excluded from analysis (left panel) and the percentages of the subpopulations of the BCSC (marked brown) and non-BCSC (marked green) in untreated (n = 4) and CAF-treated tumors (CAF-survived n = 3; CAF regrowth n = 4) (right panel). One-way ANOVA Turkey's multiple comparisons test. ****P < .001
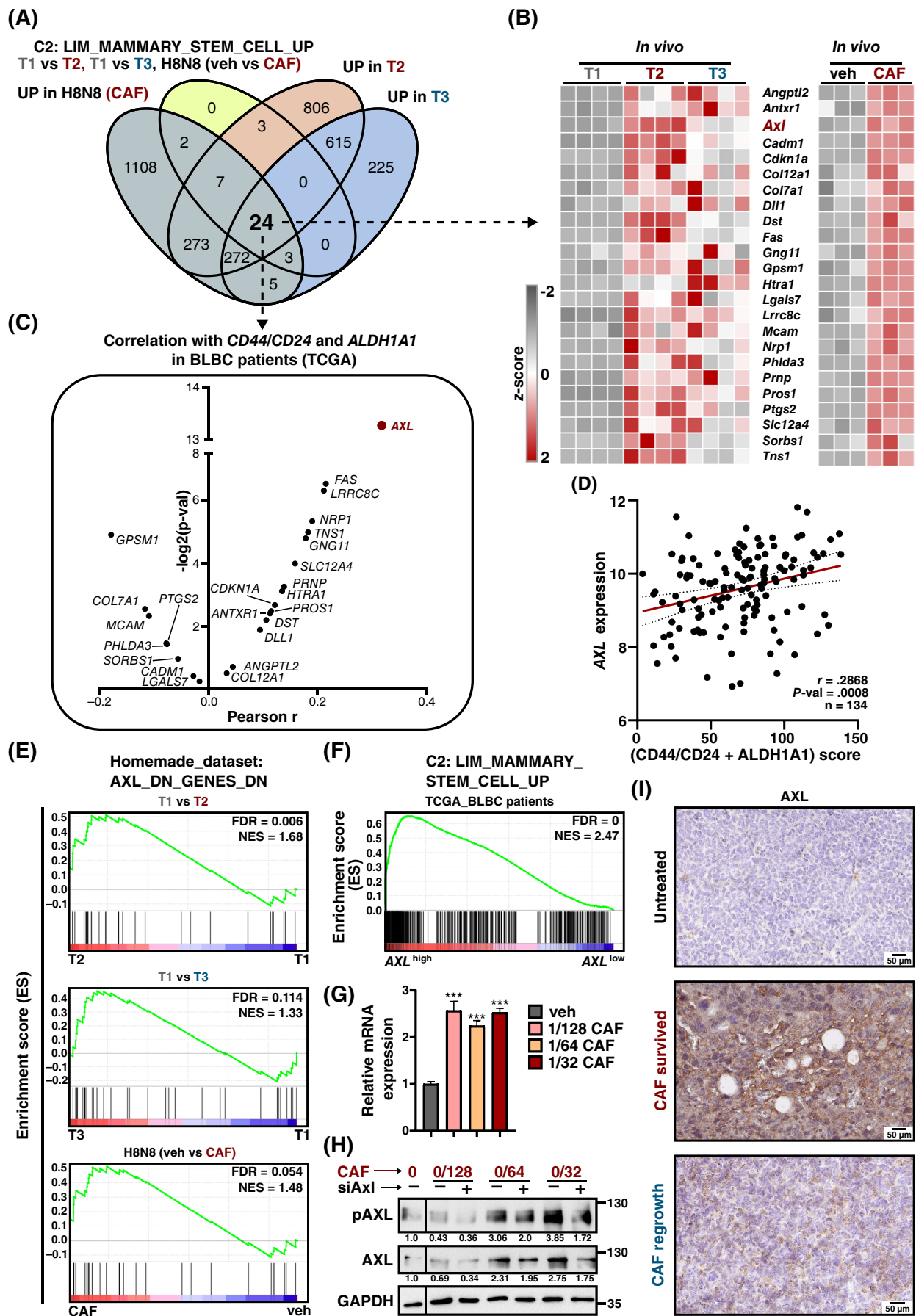
FIGURE 5 Legend on next page.

chemotherapy efficiency, we examined in more detail all significantly upregulated genes in CAF-treated H8N8 cells, CAF-survived (T2) and -regrowth (T3) tumors. Intersecting the results with known mammary-specific BCSC markers of the LIM_MAMMARY_STEM_CELL_UP gene set (MSigDB), we identified 24 commonly upregulated genes (Figure 5A,B). While estimating the stemness of BLBC-patients' lesions of the TCGA-BRCA dataset along with a (CD44/CD24/ALDH1A1) score, we noticed that the expression of the vast majority of these identified genes significantly positively correlated with this combined marker. Strikingly, we identified AXL as the top candidate gene associated with the (CD44/CD24/ALDH1A1) score in BLBC patients (Figure 5C,D). This finding was interesting as AXL is a receptor tyrosine kinase currently the focus of intensive research efforts because of its tumor-promoting function in different cancer entities.[27,28] To determine if the AXL signaling was indeed stimulated in tumor cells surviving chemotherapy, we generated a homemade AXL-specific gene set from publicly available mRNA-seq data.[29] Subsequent GSEA demonstrated that CAF-treated cells and tumors strongly enriched the AXL-dependent gene expression program (Figure 5E). In line, AXL[high] BLBC patients of the TCGA-BRCA dataset showed a pronounced enrichment of the LIM_MAMMARY_STEM_-CELL_UP gene signature (Figure 5F). We validated the induction of Axl mRNA and protein level in response to chemotherapy in H8N8 cells treated with increasing doses of CAF in vitro (Figure 5G,H). The specificity of the signal was confirmed by siRNA-mediated AXL silencing (Figures 5H and S2D). Finally, we performed immunohistochemical staining on untreated, CAF-survived and CAF-regrowth specimens. Here also, increased AXL levels were observed in tumor tissue of both chemotherapy-treated groups in comparison to controls (Figure 5I). Collectively, our data revealed AXL as an upregulated druggable factor upon the first cycle of chemotherapy and potentially implicated in the acquisition of BCSC properties as well as of drug-tolerance in BLBC.

3.6 | AXL sustains CSC properties and promotes chemotherapy tolerance in BLBC

Next, to investigate the direct implication of AXL signaling in promoting CSC properties in BLBC cells, we leveraged R428 (AXLi), a potent AXL small molecule inhibitor (Figure S3A). We performed an in vitro tumorsphere formation assay applying two concentrations of AXLi. Here, we observed a strong impairment of tumorsphere formation capacity in all AXLi-treated H8N8 cells, confirming thereby the stemness-promoting role of AXL (Figure 6A). Based on this result, we reasoned that AXLi treatment should sensitize BLBC cells to chemotherapy. Indeed, AXL inhibition (Figures 6B and S3B) or silencing (Figure S2E,F) synergized with increasing doses of CAF in H8N8 BLBC cells and robustly impaired the clonogenic capacity of CAF-treated colonies (Figure 6C). To further validate the implication of AXL signaling in stimulating resistant phenotypes in BLBC, we treated H8N8 cells with recombinant growth arrest-specific 6 (rGAS6), a specific ligand of the AXL receptor.[30] Strikingly, rGas6 treatment strongly reduced the sensitivity of the cells to CAF, as shown in a growth kinetic assay (Figure 6D). Interestingly, our mRNA-seq investigations identified Protein S (Pros1), a well-known ligand of the TAM receptor family members,[31] as highly induced in CAF-treated H8N8 cells in vitro and tumors in vivo (Figures 5A,B and 6E). Treatment of H8N8 cells with increasing doses of recombinant PROS1 (rPROS1) potentiated their drug-tolerant behavior and strongly antagonized the cytotoxic effects of CAF (Figure 6F,G). Previous studies established PROS1 as a ligand for MERTK and TYRO3,[32,33] two other members of the TAM receptor family, but reports on PROS1-mediated AXL activation are very scarce.[34] Therefore, we verified the capacity of PROS1 to induce AXL phosphorylation by treating H8N8 cells with increasing doses of rPROS1 (Figure 6H). Next, to estimate the potential implication of MERTK and TYRO3 in the induction of rPROS1-mediated therapy resistance, we had a closer look at mRNA-seq data and assessed their expression levels upon CAF therapy in tumors of our BLBC models. Noteworthy, Tyro3 was strongly downregulated in CAF-treated H8N8 cells and CAF-survived (T2) tumors whereas Mertk was mildly upregulated in CAF-survived tumors (T2) and unchanged in CAF-treated H8N8 (Figure S3C,D). Therefore, we excluded an involvement of TYRO3 and hypothesized that MERTK may be partially responsible for sustaining the PROS1-dependent drug-tolerant behavior of H8N8 cells. Surprisingly, MERTK inhibition via increasing doses of UNC2250 (MERTKi) or MERTK silencing antagonized the cytotoxic effects of CAF

FIGURE 5 AXL signaling pathway is enriched in CAF-treated tumor cells. (A) Venn diagram of the significantly upregulated genes in CAF-treated H8N8 cells, CAF-survived (T2) and CAF-regrowth (T3) BLBC cells overlapped with enriched genes from the "LIM_MAMMARY_STEM_CELL_UP" gene set in all three BLBC settings (basemean ≥10, Log$_2$FC ≥0.7, P-val <.05). (B) Heatmap of the 24 common genes from Figure 5A in vivo (untreated [T1], CAF-survived [T2], CAF-regrowth [T3]) and in vitro (vehicle and CAF-treated H8N8 cells). (C) Volcano plot showing the correlation of these 24 genes with CD44/CD24 and ALDH1A1 in BLBC patients. (D) Correlation of AXL expression with CD44/CD24 and ALDH1A1 score in BLBC patients. (E) GSEA profile showing an enrichment of the "AXL_DN_GENES_DN" signature (homemade dataset, accession number: GSE120268) in CAF-survived (T2) and CAF-regrowth (T3) compared to untreated (T1) cells, and in H8N8 cells at basal state (control) compared to CAF-treated H8N8 cells. (F) GSEA profile showing an enrichment of the "LIM_MAMMARY_STEM_CELL_UP" signature (MSigDB: C2 curated gene sets) in AXL^{high}- compared AXL^{low}-expressing BLBC patients (TCGA). NES, normalized enrichment score. (G) Increase of Axl expression in H8N8 cells upon CAF treatment, as measured via qRT-PCR. (H) Increased protein expression of AXL and phospho-Tyr773 of AXL (pAXL) upon 48 hours CAF-treatment w/ or w/o AXL knockdown, as measured via western blot. The provided densitometry values are normalized to the GAPDH signal. (I) Representative images of immunohistochemical detection of AXL in untreated, CAF-survived and CAF-regrowth tumors. Scale bars: 50 μm. Error bars: SE of the mean (SEM). (I) One-way ANOVA Turkey's multiple comparison test. ***P-val ≤.005. Student t-test: (G-I) All experiments were performed in at least biological triplicates (n ≥ 3).

(A)

H8N8 - sphere formation – R428

(B)

Dose response matrix

ZIP synergy score: 10.065

(C)

H8N8 - colony formation – R428 and CAF

(D)

H8N8 - rGAS6 and CAF

(E) *Pros1*

(F)

H8N8 - rPROS1 and CAF

(G)

Dose response matrix

ZIP synergy score: −18.154

(H)

(I)

Receiver operating characteristic
AXL(202685_s_at)

(J)
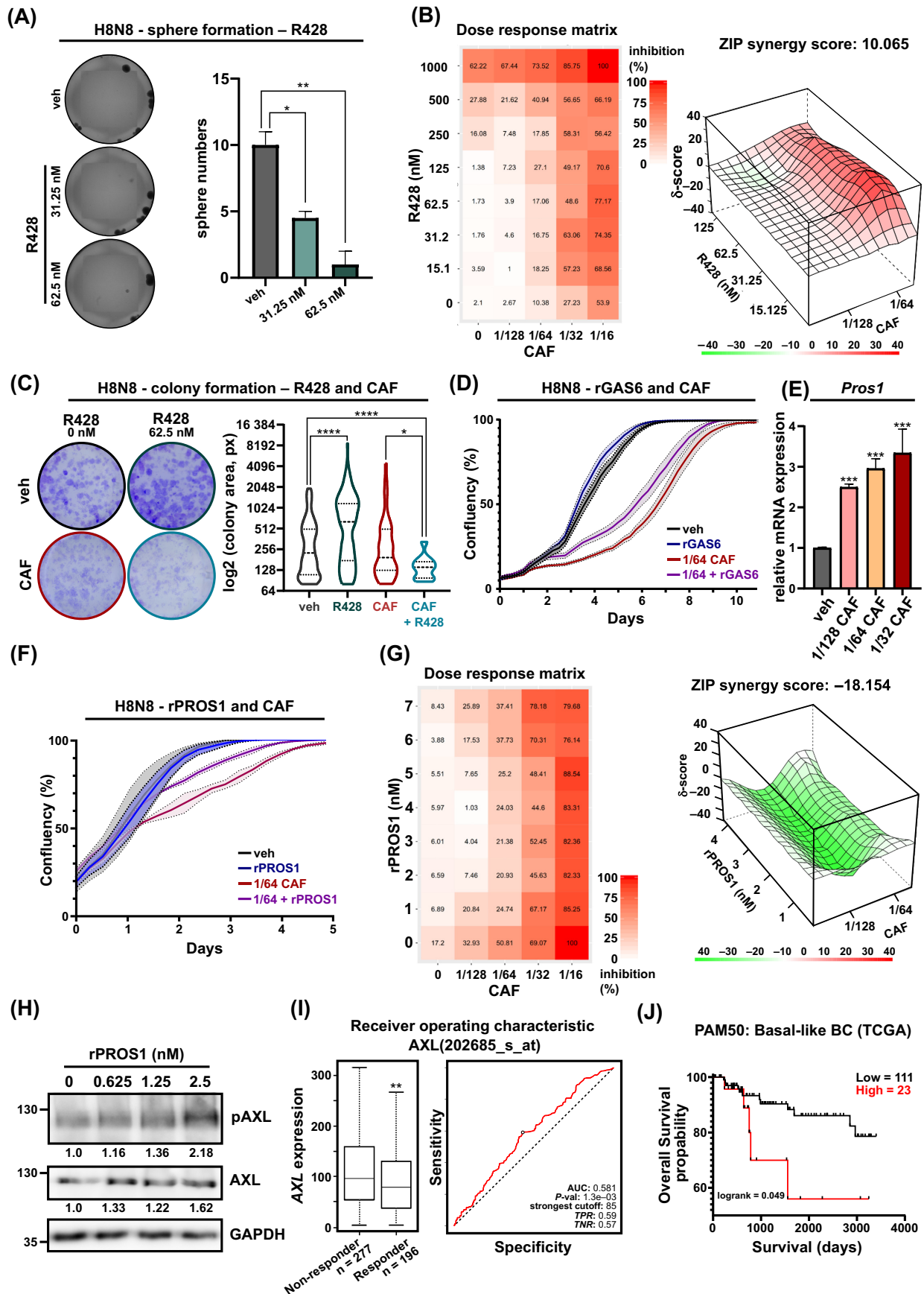
PAM50: Basal-like BC (TCGA)

FIGURE 6 Legend on next page.

(Figure S3E,F) in H8N8 cells. Hence, we concluded that PROS1 enacts its drug-resistance supporting function by stimulating the AXL-axis in BLBC cells.

Further strengthening our findings, analysis of TNBC patient data from the Receiver Operating Characteristic (ROC) database (http://www.rocplot.org/) demonstrated that patients with AXL^high lesions have a poorer response to chemotherapy than their AXL^low counterparts (Figure 6I). Accordingly, the survival of AXL^high patients was worse than AXL^low patients (dataset: TCGA-BRCA; BLBC) (Figure 6J). In summary, we identified AXL as a druggable target involved in the acquisition of stem-cell-like properties upon the establishment of a drug-tolerant state in BLBC.

4 | DISCUSSION

Recurrent cancers are highly refractory to chemotherapy, posing an urgent unmet issue in cancer treatment.[9,35] In our study, we aimed to unravel the temporal dynamics underlying the acquisition of chemoresistance in BLBC. Using a combination of magnetic tumor cell sorting and high-throughput transcriptome analyses, we demonstrate that the treatment of H8N8 tumors with a single chemotherapy dose already leads to increased therapy resistance and results in a permanent tumor cell phenotype change with the acquisition of stem cell properties through signaling of the PROS1/AXL axis.

To date, the development of a lethal chemotherapy-resistant tumor phenotype has been explained through two independent phenomena: on the one hand, it was demonstrated that repeated cytotoxic treatments lead to the selection of pre-existent more resistant clones.[36,37] On the other hand, it was shown that tumor cells under chemotherapy selective pressure experience profound transcriptional and mutational changes leading to the emergence of resistant phenotypes.[36] In an elegant study, Kim et al investigated the behavior of human TNBC composition upon chemotherapy using single-cell sequencing techniques. Approximately half of the patients showed a so-called clonal extinction whereas the other half obtained a "clonal persistence" associated with resistance.[36] In line with these results, the group of Cristofori combined the PyMT mammary carcinoma mouse model with multicolor clonal tracking and demonstrated that the different clones of endogenous growing tumors do not equally respond to chemotherapy treatment. Surprisingly, fast-growing clones were more efficiently surviving the cytotoxic regimen.[37] These two studies and others demonstrate the complexity of the processes ruling the emergence of drug-tolerant lesions in multiclonal breast cancers. Although certainly largely overlapping, strategies developed by different surviving clones are unique, rendering their studies in multiclonal lesion systems, particularly challenging. Our approach using the H8N8 cell line implanted in syngeneic recipients intended to reduce this complexity in an immunocompetent in vivo setting. Interestingly, a further in vivo study by Echeverria et al on TNBC patient-derived xenograft confirmed the persistence of clonal heterogeneity after cytotoxic treatment. However, although their treatment strategy was very close to ours, their results pointed at a reversible drug-tolerant state of the tumor cells.[38] In contrast, we demonstrate that even if the phenotype of tumors regrowing after a cycle of chemotherapy reverted to one close to the untreated one, these lesions already displayed increased drug resistance even after several passages in the cell culture, as assessed in our retransplantation study. The implication of stem cell properties and phenotypic plasticity in breast cancer drug resistance has been proposed over a decade ago and was confirmed later in multiple other studies.[11,39-43] Surprisingly, chemotherapy-surviving cancer cells analyzed by Echeverria et al did not enrich these gene expression profiles, underlining the variety of mechanisms leveraged during the process of drug resistance acquisition.[38] Under this aspect, treatments sensitizing cancer cells to cytotoxic drugs without affecting the acquisition of stem cell features may allow for a switch to other resistance strategies. This assumption is supported by Jewer et al, who revealed that mTOR signaling activated by hypoxic stress unexpectedly induces breast cancer cell plasticity like chemotherapy-triggered stress.[44] Since our study revealed a fast kinetic of stemness properties accumulation after the first cycle of CAF treatment, supplementation with therapies impairing the acquisition of such properties should be already considered during first-line treatments. For instance, the expansion of the BCSC could be prohibited by targeting the CD44+CD24− population of TNBC lesions, as proposed by Marangoni et al.[45] In this elegant study, the authors efficiently prevented tumor

---

FIGURE 6 AXL is decisive for promoting a stemness-driven chemotherapy resistance phenotype and its expression is associated with a poor prognosis in TNBC patients. (A) Tumorsphere formation assay in H8N8 cells upon different concentrations of AXL kinase inhibition (R428). (B) Heatmap matrix of dose-dependent response percentage (left panel) and 3D-synergy landscape (right panel) to increasing doses of R428 and CAF showing synergy of both compounds in H8N8 BLBC cells. (C) Crystal violet staining of colonies in 1/64 CAF-treated H8N8 cells upon R428 treatment (left panel) and their quantification (right panel). (D) Proliferation assay of 1/64 CAF-treated H8N8 cells upon treatment with recombinant protein GAS6 (rGAS6). (E) qRT-PCR of *Pros1* in H8N8 cells upon CAF treatment. (F) Proliferation assay of H8N8 cells treated with 1/64 CAF and recombinant PROS1 (rPROS1, for 24 hours). (G) Heatmap matrix of dose-dependent response percentage (left panel) and 3D-antagonism landscape (right panel) to increasing doses of rPROS1 (for 24 hours) and CAF showing an antagonism of both compounds; rPROS1 potentiates the survival of H8N8 BLBC towards increasing doses of CAF. (H) Protein expression of phospho-Tyr773 of AXL (pAXL) and total AXL to increasing doses of rPROS1 (for 24 hours), as assessed by western blotting. The provided densitometry values are normalized to the GAPDH signal. (I) ROC analysis from publically available TNBC data demonstrates that patients with poor response to chemotherapy harbor high expression levels of *AXL*. Box plots: Mann-Whitney test. AUC, area under the curve; TPR, true positive rate; TNR, true negative rate. (J) Kaplan-Meier plots showing the overall survival probability of *AXL*-expressing BLBC patients (expression and survival data are from the TCGA-BRCA database). Log-rank test. All experiments were performed in biological triplicates. (A, C, D, E and F) One-way ANOVA Turkey's multiple comparisons test. *P-val <.05, **P-val <.01, ***P-val <.005, ****P-val <.001

regrowth by combining a doxorubicin/cyclophosphamide chemotherapy with the monoclonal antibody P245 directed against the cell surface receptor CD44. However, impairing the outgrowth of the BCSC compartment is likely a very challenging task as this cell population was shown to harbor a certain heterogeneity with a CD44$^+$CD24$^-$ phenotype preferentially localized at the periphery whereas BCSC in more central areas of the tumor rather displays high ALDH activity.[46] Here, additional use of ALDH inhibitors proposed by Croker and Allan could also help to increase or at least maintain constant chemotherapy efficiency throughout the consecutive cycles of treatment.[47]

Following an extended unbiased data-mining approach, we identified AXL as a top CSC-associated marker that potentiates drug tolerance in BLBC recurrences. Through its capacity to stimulate oncogenic PI3K-AKT-mTOR, MAPK, JAK-STAT and SRC-FAK signaling, AXL can sustain aberrant stem cell renewal, epithelial-to-mesenchymal transition (EMT), immune evasion and cancer cell invasion.[48,49] Particularly in normal and tumor cells of the mammary gland, AXL was frequently shown to play a critical role in the maintenance of stem cell properties.[48,50-52] Inline, several reports suggested an implication of the AXL signaling in drug-resistant phenotypes of TNBC. Wilson et al identified R428 synergizing with antimitotic agents in resistant cell lines.[51] In a later study, R428 was also found to synergize with Auranofin, a thioredoxin reductase inhibitor inducing cancer cell apoptosis.[53] Additionally, the group of Santarpia reported that relapsing TNBCs upregulated AXL to polarize macrophages into the M2-like tumor-supportive phenotype, increasing thereby their resistance to the therapy.[54] Our sequential analysis of in vivo chemotherapy resistance acquisition align with these reports, revealing for the first time AXL as a very early and central player in the process of acquisition of chemotherapy resistance. Interestingly, our findings demonstrated that a sole stimulation of AXL signaling through rGAS6 or rPROS1 treatment was sufficient to induce chemoresistant phenotypes. A similar tumor cell survival-promoting role was also observed in chemotherapy-treated prostate cancer.[55] Oppositely, interference of GAS6-AXL interaction through low doses of Warfarin blocked the progression, spreading and therapy resistance of pancreatic tumors.[56] In line, a very recent study by Mullen et al on ovarian cancer demonstrated a strong sensitization to chemotherapy and Poly (ADP-ribose) polymerase (PARP)-inhibition through AVB-500 meditated GAS6 neutralization.[57] Furthermore, a recent study from Hirokazu et al demonstrated that tumor-associated macrophages-secreted PROS1 functions as a ligand of AXL to sustain the aggressive properties of glioma sphere cultures and that their expression is strongly correlated with poor survival outcomes for glioblastoma multiforme patients.[34] In the present story, we show that loss of AXL signaling through siRNA interference or the small molecule inhibitor Bemcentinib (R428) efficiently impaired the capacity of BLBC cells to survive conventional cytotoxic chemotherapy, thereby identifying AXL as a druggable target to sensitize cancer cells to cytotoxic drugs.

Although the germline inactivation of several receptors leads to embryonic lethality, Axl^{KO} mice are viable and fertile.[58] Recently, Engelsen et al showed that Axl^{KO} mice did not exhibit any sign of mammary stem cell renewal impairment. However, orthotopic transplantation of Axl^{KO} mammary epithelial cells into clear fat pads of recipient

prepubescent mice was able to compromise the mammary gland reconstitution, indicating the central importance of this receptor in regenerative or wound healing processes.[48] Hence, promising future AXL-targeting therapies are expected to show high anticancer properties with rather low toxicity for the patients, especially when combining conventional chemotherapy with AXL inhibition to prevent evolution to resistant phenotypes.

Concluding, our in vivo study identified AXL signaling as an early event in therapy resistance acquisition in BLBC already occurring upon one single chemotherapy dose. Strategies specifically blocking protumorigenic programs should therefore be considered already at the very early treatment stage. This work establishes AXL as a very promising therapeutic target to optimize currently used chemotherapies in BLBC patients by reducing chemoresistance.

AUTHOR CONTRIBUTIONS

Garyfallia Pantelaiou-Prokaki: Performed cell culture experiments; Data analysis; Analyzed publically available data; Designed figures and wrote the article supported by FW and FA and the input of the co-authors. **Oliver Reinhardt:** Designed the study with input from WD; performed cell culture experiments; Performed tumor cell dissociation and singe-cell sorting for next-generation sequencing; Performed mRNA-seq library preparation; Performed mouse experiments; Carried out and analyzed histological analyses; Designed figures and wrote the article supported by FW and FA and the input of the co-authors. **Nadine S. Georges:** Performed cell culture experiments. **David J. Agorku:** Performed tumor cell dissociation and singe-cell sorting for next-generation sequencing; dissociated tumor samples, isolated tumor cells and established cell lines. **Olaf Hardt:** Designed the study with input from WD; Performed tumor cell dissociation and singe-cell sorting for next-generation sequencing. **Evangelos Prokakis:** Analyzed publically available data; Designed figures and wrote the article supported by FW and FA and the input of the co-authors. **Iga K. Mieczkowska:** Performed mRNA-seq library preparation. **Wolfgang Deppert:** Provided input. **Florian Wegwitz:** Designed the study with input from WD; Performed mRNA-seq library preparation. **Frauke Alves:** Designed the study with input from WD. All authors reviewed and approved this article. The work reported in the article has been performed by the authors, unless specified in the text.

"Unravelling epigenetic mechanisms of CAF-chemotherapy resistance in mammary carcinoma" to FW.

CONFLICT OF INTEREST

The authors declare no conflicts of interest.

DATA AVAILABILITY STATEMENT

All mRNA-seq data of H8N8 cells (in vitro) and T1 (untreated), T2 (CAF-survived) and T3 (CAF-regrowth) cells (in vivo) have been deposited at ArrayExpress (http://www.ebi.ac.uk/arrayexpress), under the accession numbers E-MTAB-11344 and E-MTAB-9589, respectively. Other data that support the findings of our study are available from the corresponding author upon request.

ETHICS STATEMENT

Our study was conducted in accordance with German regulations for animal experiments (Niedersächsisches Landesamt für Verbraucherschutz und Lebensmittelsicherheit, LAVES, ethics approval no. 33.19-42 502-04-16/1621) entitled "Therapiewirkung im Mammakarzinom Mausmodell."

ORCID

Garyfallia Pantelaiou-Prokaki https://orcid.org/0000-0002-1954-4919

Olaf Hardt https://orcid.org/0000-0003-0825-071X
Evangelos Prokakis https://orcid.org/0000-0001-9297-1821
Iga K. Mieczkowska https://orcid.org/0000-0002-3684-3945
Florian Wegwitz https://orcid.org/0000-0003-0750-6998
Frauke Alves https://orcid.org/0000-0002-6258-5409

REFERENCES

1. Harbeck N, Penault-Llorca F, Cortes J, et al. Breast cancer. *Nat Rev Dis Primers*. 2019;5:66.
2. Lebert JM, Lester R, Powell E, Seal M, McCarthy J. Advances in the systemic treatment of triple-negative breast cancer. *Curr Oncol*. 2018;25:S142-S150.
3. Carey LA, Dees EC, Sawyer L, et al. The triple negative paradox: primary tumor chemosensitivity of breast cancer subtypes. *Clin Cancer Res*. 2007;13:2329-2334.
4. Gerber B, Freund M, Reimer T. Recurrent breast cancer: treatment strategies for maintaining and prolonging good quality of life. *Dtsch Arztebl Int*. 2010;107:85-91.
5. Nunnery SE, Mayer IA, Balko JM. Triple-negative breast cancer: breast tumors with an identity crisis. *Cancer J*. 2021;27:2-7.
6. Nedeljković M, Damjanović A. Mechanisms of chemotherapy resistance in triple-negative breast cancer-how we can rise to the challenge. *Cells*. 2019;8:957.
7. Lee KL, Kuo YC, Ho YS, Huang YH. Triple-negative breast cancer: current understanding and future therapeutic breakthrough targeting cancer stemness. *Cancers (Basel)*. 2019;11:1334.
8. Park SY, Choi JH, Nam JS. Targeting cancer stem cells in triple-negative breast cancer. *Cancers (Basel)*. 2019;11(7):965.
9. Boumahdi S, de Sauvage FJ. The great escape: tumour cell plasticity in resistance to targeted therapy. *Nat Rev Drug Discov*. 2020;19:39-56.
10. Scioli MG, Storti G, D'amico F, et al. The role of breast cancer stem cells as a prognostic marker and a target to improve the efficacy of breast cancer therapy. *Cancers (Basel)*. 2019;11(7):1021.
11. Ginestier C, Hur MH, Charafe-Jauffret E, et al. ALDH1 is a marker of normal and malignant human mammary stem cells and a predictor of poor clinical outcome. *Cell Stem Cell*. 2007;1:555-567.
12. Lima JF, Nofech-Mozes S, Bayani J, Bartlett JMS. EMT in breast carcinoma—a review. *J Clin Med*. 2016;5(7):65.
13. Kotiyal S, Bhattacharya S. Breast cancer stem cells, EMT and therapeutic targets. *Biochem Biophys Res Commun*. 2014;453:112-116.
14. Zhou S, Schuetz JD, Bunting KD, et al. The ABC transporter Bcrp1/ABCG2 is expressed in a wide variety of stem cells and is a molecular determinant of the side-population phenotype. *Nat Med*. 2001;7:1028-1034.
15. Maenz C, Lenfert E, Pantel K, Schumacher U, Deppert W, Wegwitz F. Epithelial-mesenchymal plasticity is a decisive feature for the metastatic outgrowth of disseminated WAP-T mouse mammary carcinoma cells. *BMC Cancer*. 2015;15:1-10.
16. Lenfert E, Maenz C, Heinlein C, et al. Mutant p53 promotes epithelial-mesenchymal plasticity and enhances metastasis in mammary carcinomas of WAP-T mice. *Int J Cancer*. 2015;136:E521-E533.
17. Jannasch K, Dullin C, Heinlein C, et al. Detection of different tumor growth kinetics in single transgenic mice with oncogene-induced mammary carcinomas by flat-panel volume computed tomography. *Int J Cancer*. 2009;125:62-70.
18. Otto B, Gruner K, Heinlein C, et al. Low-grade and high-grade mammary carcinomas in WAP-T transgenic mice are independent entities distinguished by met expression. *Int J Cancer*. 2013;132:1300-1310.
19. Wegwitz F, Kluth MA, Mänz C, et al. Tumorigenic WAP-T mouse mammary carcinoma cells: a model for a self-reproducing homeostatic cancer cell system. *PLoS One*. 2010;5:e12103.
20. Mieczkowska IK, Pantelaiou-Prokaki G, Prokakis E, et al. Decreased PRC2 activity supports the survival of basal-like breast cancer cells to cytotoxic treatments. *Cell Death Dis*. 2021;12:1118.
21. Pantelaiou-Prokaki G, Mieczkowska I, Schmidt GE, et al. HDAC8 suppresses the epithelial phenotype and promotes EMT in chemotherapy-treated basal-like breast cancer. *Clin Epigenetics*. 2022;14:14.
22. Jannasch K, Wegwitz F, Lenfert E, Maenz C, Deppert W, Alves F. Chemotherapy of WAP-T mouse mammary carcinomas aggravates tumor phenotype and enhances tumor cell dissemination. *Int J Cancer*. 2015;137:25-36.
23. Schulze-Garg C, Löhler J, Gocht A, Deppert W. A transgenic mouse model for the ductal carcinoma in situ (DCIS) of the mammary gland. *Oncogene*. 2000;19:1028-1037.
24. Prokakis E, Dyas A, Grün R, et al. USP22 promotes HER2-driven mammary carcinoma aggressiveness by suppressing the unfolded protein response. *Oncogene*. 2021;40:4004-4018.
25. Wegwitz F, Prokakis E, Pejkovska A, et al. The histone H2B ubiquitin ligase RNF40 is required for HER2-driven mammary tumorigenesis. *Cell Death Dis*. 2020;11:873.
26. Marzagalli M, Fontana F, Raimondi M, Limonta P. Cancer stem cells—key players in tumor relapse. *Cancers (Basel)*. 2021;13:1-23.
27. Scherschinski L, Prem M, Kremenetskaia I, et al. Regulation of the receptor tyrosine kinase AXL in response to therapy and its role in therapy resistance in glioblastoma. *Int J Mol Sci*. 2022;23(2):982.
28. Du W, Phinney NZ, Huang H, et al. AXL is a key factor for cell plasticity and promotes metastasis in pancreatic cancer. *Mol Cancer Res*. 2021;19:1412-1421.
29. Goyette MA, Cusseddu R, Elkholi I, et al. AXL knockdown gene signature reveals a drug repurposing opportunity for a class of antipsychotics to reduce growth and metastasis of triple-negative breast cancer. *Oncotarget*. 2019;10:2055-2067.
30. Varnum BC, Young C, Elliott G, et al. Axl receptor tyrosine kinase stimulated by the vitamin K-dependent protein encoded by growth-arrest-specific gene 6. *Nature*. 1995;373:623-626.
31. Burstyn-Cohen T. TAM receptor signaling in development. *Int J Dev Biol*. 2017;61:215-224.

32. Tsou WI, Nguyen KQN, Calarese DA, et al. Receptor tyrosine kinases, TYRO3, AXL, and MER, demonstrate distinct patterns and complex regulation of ligand-induced activation. *J Biol Chem*. 2014;289: 25750-25763.

33. Graham DK, Deryckere D, Davies KD, Earp HS. The TAM family: phosphatidylserine-sensing receptor tyrosine kinases gone awry in cancer. *Nat Rev Cancer*. 2014;14:769-785.

34. Sadahiro H, Kang KD, Gibson JT, et al. Activation of the receptor tyrosine kinase AXL regulates the immune microenvironment in glioblastoma. *Cancer Res*. 2018;78:3002-3013.

35. Hancock BA, Chen YH, Solzak JP, et al. Profiling molecular regulators of recurrence in chemorefractory triple-negative breast cancers. *Breast Cancer Res*. 2019;21:87.

36. Kim C, Gao R, Sei E, et al. Chemoresistance evolution in triple-negative breast cancer delineated by single-cell sequencing. *Cell*. 2018;173:879-893.e13.

37. Tiede S, Kalathur RKR, Lüönd F, et al. Multi-color clonal tracking reveals intra-stage proliferative heterogeneity during mammary tumor progression. *Oncogene*. 2021;40:12-27.

38. Echeverria GV, Ge Z, Seth S, et al. Resistance to neoadjuvant chemotherapy in triple-negative breast cancer mediated by a reversible drug-tolerant state. *Sci Transl Med*. 2019;11(488):eaav0936.

39. Li QQ, Da XJ, Wang WJ, et al. Twist1-mediated adriamycin-induced epithelial-mesenchymal transition relates to multidrug resistance and invasive potential in breast cancer cells. *Clin Cancer Res*. 2009;15: 2657-2665.

40. Charafe-Jauffret E, Ginestier C, Iovino F, et al. Aldehyde dehydrogenase 1-positive cancer stem cells mediate metastasis and poor clinical outcome in inflammatory breast cancer. *Clin Cancer Res*. 2010;16: 45-55.

41. Li X, Lewis MT, Huang J, et al. Intrinsic resistance of tumorigenic breast cancer cells to chemotherapy. *J Natl Cancer Inst*. 2008;100: 672-679.

42. Creighton CJ, Li X, Landis M, et al. Residual breast cancers after conventional therapy display mesenchymal as well as tumor-initiating features. *Proc Natl Acad Sci U S A*. 2009;106:13820-13825.

43. Elbaiomy MA, Akl T, Atwan N, Elsayed AA, Elzaafarany M, Shamaa S. Clinical impact of breast cancer stem cells in metastatic breast cancer patients. *J Oncol*. 2020;2020:1-8.

44. Jewer M, Lee L, Leibovitch M, et al. Translational control of breast cancer plasticity. *Nat Commun*. 2020;11:1-16.

45. Marangoni E, Lecomte N, Durand L, et al. CD44 targeting reduces tumour growth and prevents post-chemotherapy relapse of human breast cancers xenografts. *Br J Cancer*. 2009;100:918-922.

46. Liu S, Cong Y, Wang D, et al. Breast cancer stem cells transition between epithelial and mesenchymal states reflective of their normal counterparts. *Stem Cell Rep*. 2014;2:78-91.

47. Croker AK, Allan AL. Inhibition of aldehyde dehydrogenase (ALDH) activity reduces chemotherapy and radiation resistance of stem-like ALDH hiCD44 + human breast cancer cells. *Breast Cancer Res Treat*. 2012;133:75-87.

48. Engelsen AST, Wnuk-Lipinska K, Bougnaud S, et al. AXL is a driver of stemness in normal mammary gland and breast cancer. *iScience*. 2020;23(11):101649.

49. Scaltriti M, Elkabets M, Baselga J. Molecular pathways: AXL, a membrane receptor mediator of resistance to therapy. *Clin Cancer Res*. 2016;22:1313-1317.

50. Khera L, Vinik Y, Maina F, Lev S. The AXL-PYK2-PKCα axis as a nexus of stemness circuits in TNBC. *Life Sci Alliance*. 2021;4:1-17.

51. Wilson C, Ye X, Pham T, et al. AXL inhibition sensitizes mesenchymal cancer cells to antimitotic drugs. *Cancer Res*. 2014;74:5878-5890.

52. Shen Y, Zhu Q, Xiao M, et al. Inhibitory effect of the novel tyrosine kinase inhibitor DCC-2036 on triple-negative breast cancer stem cells through AXL-KLF5 positive feedback loop. *Cell Death Dis*. 2022;13(8):749.

53. Ryu YS, Shin S, An HG, et al. Synergistic induction of apoptosis by the combination of an axl inhibitor and auranofin in human breast cancer cells. *Biomol Ther*. 2020;28:473-481.

54. Bottai G, Raschioni C, Székely B, et al. AXL-associated tumor inflammation as a poor prognostic signature in chemotherapy-treated triple-negative breast cancer patients. *npj Breast Cancer*. 2016;2:16033.

55. Lee E, Decker AM, Cackowski FC, et al. Growth arrest-specific 6 (GAS6) promotes prostate cancer survival by G1 arrest/S phase delay and inhibition of apoptosis during chemotherapy in bone marrow. *J Cell Biochem*. 2016;117:2815-2824.

56. Kirane A, Ludwig KF, Sorrelle N, et al. Warfarin blocks Gas6-mediated Axl activation required for pancreatic cancer epithelial plasticity and metastasis. *Cancer Res*. 2015;75:3699-3705.

57. Mullen MM, Lomonosova E, Toboni MD, et al. GAS6/AXL inhibition enhances ovarian cancer sensitivity to chemotherapy and PARP inhibition through increased DNA damage and enhanced replication stress. *Mol Cancer Res*. 2022;20:265-279.

58. Lu Q, Gore M, Zhang Q, et al. Tyro-3 family receptors are essential regulators of mammalian spermatogenesis. *Nature*. 1999;398:723-728.

SUPPORTING INFORMATION

Additional supporting information can be found online in the Supporting Information section at the end of this article.